Molecular Cell 24, 267–278, October 20, 2006 ©2006 Elsevier Inc. DOI 10.1016/j.molcel.2006.08.021

Organization of Core Spliceosomal Components U5 snRNA Loop I and U4/U6 Di-snRNP within U4/U6.U5 Tri-snRNP as Revealed by Electron Cryomicroscopy

Bjoern Sander,[1] Monika M. Golas,[1] Evgeny M. Makarov,[1,2,3] Hero Brahms,[1,4] Berthold Kastner,[1] Reinhard Lührmann,[1,*] and Holger Stark[1,*]

[1] Max Planck Institute for Biophysical Chemistry
[2] Department of Cellular Biochemistry
Am Fassberg 11
37077 Göttingen
Germany

Summary

In eukaryotes, pre-mRNA exons are interrupted by large noncoding introns. Alternative selection of exons and nucleotide-exact removal of introns are performed by the spliceosome, a highly dynamic macromolecular machine. U4/U6.U5 tri-snRNP is the largest and most conserved building block of the spliceosome. By 3D electron cryomicroscopy and labeling, the exon-aligning U5 snRNA loop I is localized at the center of the tetrahedrally shaped tri-snRNP reconstructed to ~2.1 nm resolution in vitrified ice. Independent 3D reconstructions of its subunits, U4/U6 and U5 snRNPs, show how U4/U6 and U5 combine to form tri-snRNP and, together with labeling experiments, indicate a close proximity of the spliceosomal core components U5 snRNA loop I and U4/U6 at the center of tri-snRNP. We suggest that this central tri-snRNP region may be the site to which the prespliceosomal U2 snRNA has to approach closely during formation of the catalytic core of the spliceosome.

Introduction

Alternative splicing of premessenger RNA (pre-mRNA) makes a central contribution to eukaryotic protein diversity and is accomplished by the spliceosome, a remarkably complex macromolecular machine (Will and Lührmann, 2006). The spliceosome removes noncoding introns from newly synthesized pre-mRNA and joins the coding exon segments together in a two-step transesterification reaction. The splice sites (SSs) on the pre-mRNA are selected and arranged within the earliest assembly intermediates of the spliceosome: evidence has accumulated that, already in the first assembly step, the E complex, the three important pre-mRNA sites (5′ SS, branch site region, 3′ SS) are organized in close proximity (Kent and MacMillan, 2002; Kent et al., 2005). The E complex is converted into the prespliceosome (A complex) by the stable association of the U2 small nuclear ribonucleoprotein (snRNP) (Das et al., 2000) with U1 snRNP, pre-mRNA, and additional protein factors (Bennett et al., 1992; Hartmuth et al., 2002). The A complex, however, is not catalytically active by itself but requires binding of another constitutive component of the spliceosome, namely the snRNP trimer U4/U6.U5 (tri-snRNP), for catalytic core formation. The tri-snRNP (Behrens and Lührmann, 1991) is the largest and most highly conserved building block of the spliceosome. Tri-snRNP contains the two snRNP particles U5 and U4/U6, each possessing characteristic snRNA molecules and various proteins, and is central to splicing: in the catalytic core of the spliceosome, U6 snRNA base pairs with pre-mRNA and the prespliceosomal U2 snRNA and is located in close proximity to the U5 snRNA loop I (McConnell and Steitz, 2001). The spliceosome's catalytic center is thus believed to form at the interface between tri-snRNP and A complex: tri-snRNP binds to the A complex within the spliceosomal complex B and subsequently, during activation of the spliceosome, is remodeled in a series of extensive rearrangement steps (Staley and Guthrie, 1998). Among these, the U4/U6 snRNA duplex is unwound, U1 and U4 snRNPs dissociate, and the U6 snRNA base pairs instead with U2 snRNA and the 5′ SS (Wu and Manley, 1991). While base-pairing of the U2 and U6 snRNAs is considered to be essential for the catalytic core of the spliceosome, the U4 snRNA very probably only fulfils a chaperone function, thereby protecting the U6 snRNA prior to activation of the spliceosome (Staley and Guthrie, 1998).

The tri-snRNP U5 snRNA has been proposed to tether the two exon ends in the orientation needed for the second catalytic step of splicing, through its 11 nucleotide loop I, which is located very close to the catalytic center (McConnell and Steitz, 2001; Sontheimer and Steitz, 1993; Wyatt et al., 1992). The tri-snRNP harbors the large hPrp8 protein, which in the spliceosome interacts with all the important sites of the pre-mRNA, including the 5′ and 3′ SS regions and part of the polypyrimidine tract (Teigelkamp et al., 1995). It has been shown to crosslink with U5 snRNA nucleotides of loop I as well as of a uridine within the internal loop I (IL1, compare also Figure 6A) that is located close to the 5′ end of the U5 snRNA (Urlaub et al., 2000). HPrp8p has been demonstrated to bind stably to the U5-116K protein (Achsel et al., 1998), the yeast ortholog of which (Snu114p) has likewise been shown to crosslink to the U5 snRNA (Dix et al., 1998).

For many years, it has been accepted that the spliceosome undergoes dramatic structural rearrangements upon its activation; however, little is known about the structural organization of the early assembly stages of the pre-mRNA-splicing machinery at the level of its components. Recent cryo-EM studies have provided structural insights into spliceosomal complexes at different assembly stages (Azubel et al., 2004; Boehringer et al., 2004; Golas et al., 2005; Jurica et al., 2004); however, data that allow the localization of the catalytic core are not available yet because of inadequate resolution and too little information from "flagging" by specific labeling. In the precatalytic spliceosome, the tri-snRNP is bound to the prespliceosome and additional spliceosomal protein factors. It consists of a main triangular body to

*Correspondence: hstark1@gwdg.de (H.S.), reinhard.luehrmann@mpi-bpc.gwdg.de (R.L.)
[3] Present address: Department of Biochemistry, University of Leicester, Lancaster Road, Leicester LE1 9HN, United Kingdom.
[4] Present address: DRG Instruments GmbH, Frauenbergstrasse 18, 35039 Marburg, Germany.

which a large globular domain is flexibly attached (Boehringer et al., 2004). However, this 3D structure raised the question of where the catalytic core of the spliceosome would form. Several possibilities could be envisaged: for example, the catalytic core of the spliceosome could be located somewhere within the flexible domain, in the interface between flexible and triangular domain, or within the triangular domain.

Here, we determined the 3D structure of the tri-snRNP by performing 3D electron cryomicroscopy on human tri-snRNPs and its two major subunits, U5 snRNP and U4/U6 di-snRNP, localized both subunits within the tri-snRNP 3D structure, and located the U5 snRNA loop I by affinity labeling. We adduce evidence for a close spatial relationship between the two core components U5 snRNA loop I and U4/U6 di-snRNP in the tri-snRNP. Our results show how the U5 snRNP and U4/U6 di-snRNP are organized in tri-snRNP, and they indicate that the emerging spliceosomal catalytic core is located within the triangular body of the precatalytic spliceosome.

Results

3D Structure of Unstained U4/U6.U5 Tri-snRNP in Vitrified Ice

The tri-snRNP, U5 snRNP, and U4/U6 di-snRNP particles used for 3D electron cryomicroscopy were purified from HeLa nuclear extract (Behrens and Lührmann, 1991) by using immunoaffinity chromatography with a monoclonal antibody (H-20) directed against the snRNA-specific trimethylguanosine (m_3G) cap (Bochnig et al., 1987) followed by further separation on glycerol gradients. Before imaging unstained tri-snRNPs in vitrified ice (Adrian et al., 1984), the sample was transferred to a glycerol-free buffer for optimal high-contrast conditions (for a complete procedural flow chart, see Figure S1 in the Supplemental Data available with this article online). Tri-snRNPs obtained after ultracentrifugation contain the three snRNA molecules U4, U5, and U6 and 29 distinct proteins (Figure 1A) (Makarov et al., 2002), amounting to a total mass of ~1.8 MDa. Unstained cryo-EM images in vitrified buffer revealed a monodisperse population of elongated, triangular particles with a maximum dimension of ~300 Å. Owing to the strong signal of the raw images recorded under optimized conditions on a CCD camera (2-fold binning, magnification 122,000-fold) (Sander et al., 2005), a wealth of fine-structural detail is seen in the individual particles (Figure 1B).

The tri-snRNP 3D structure was calculated from ~124,000 defocus-corrected particles and refined to ~19–24 Å resolution as measured by Fourier-shell correlation (FSC) (Harauz and van Heel, 1986) (Figure 1B, inset). It exhibits an elongated, roughly tetrahedral shape with dimensions of ~305 Å × 200 Å × 175 Å (Figure 1C). The broad part of the complex (upper region in Figure 1C, panels 1 and 2) exhibits a maximum diameter of ~200 Å and is divided into two parts by a cleft. It includes a roughly annular domain, which we term the head, that is joined by thin density elements to the main body (Figure 1C, third view). The body forms a network of multiply connected domains and tapers off toward the slim, pointed lower end of the complex called foot.

3D Reconstruction of Tri-snRNP by Cryonegative Staining

A 3D reconstruction of the tri-snRNP using cryoimages negatively stained with uranyl formate (Golas et al., 2003) was refined independently of the 3D structure based on unstained images described above. The two reconstructions, stained and unstained, were practically identical, as shown in Figure S2; the consistency of the 3D structures obtained from the two types of specimen supports the assertion of their reliability. This point is especially important with respect to the isolated subunits U5 and U4/U6 snRNPs, whose 3D structures were determined by negative staining. For these, negative staining was essential since sample concentration, homogeneity, and image contrast were significantly lower than that of purified tri-snRNPs (scaled class averages of the tri-snRNP and its subunits are depicted in Figure 1D). Image processing for each of the three particles was performed independently of the others, and at no point were any results for one structure used to help refine another.

Analysis of Isolated U5 snRNPs and U4/U6 Di-snRNPs

Isolated U5 snRNPs purified by H-20 immunoaffinity chromatography followed by glycerol-gradient ultracentrifugation under low-salt conditions (150 mM NaCl) contain the U5-specific proteins hPrp8p/220K, hBrr2p/200K, 116K, hPrp6p/102K, hPrp28p/100K, 40K, and 15K as well as the 52K protein that is absent from tri-snRNP (Laggerbauer et al., 2005) and the U5 snRNA-associated set of seven common Sm proteins B/B′, D1, D2, D3, E, F, and G (Figure 2A). Thus, the U5 snRNP contributes ~60% of the total mass of the tri-snRNP. Under high-salt conditions (800 mM NaCl), the hPrp28p/100K protein is absent from the U5 snRNP (Figure 2B) (Makarov et al., 2000). To obtain U4/U6 di-snRNPs, tri-snRNPs were dissociated into the U5 and U4/U6 subunits and applied to centrifugation gradients. Isolated U4/U6 di-snRNPs (~30% of the tri-snRNP mass) contained all the U4/U6-specific proteins (90K, 61K, 60K, 20K, and 15.5K), the set of U4 snRNA-associated Sm proteins, and the U6 snRNA-associated set of hLSm proteins (Figure 2C).

EM images of U5 snRNPs purified under low-salt and high-salt conditions showed elongated particles of ~265 Å maximum diameter, with very similar main views (Figures 2D and 2E). Both U5 snRNPs are convex-concave shaped (i.e., convex on one side and concave on the opposite side) with a globular foot domain at one end (the lower domain in the class averages shown in the insets). Thus, isolated U5 snRNPs showed a maximum diameter slightly smaller than that of the tri-snRNP. In contrast, electron microscopy of isolated U4/U6 di-snRNP revealed considerably smaller particles of ~190 Å maximum diameter. In the class averages (Figure 2F), a central constriction becomes visible that leads to a bipartite appearance in the 3D reconstruction (see below).

3D Structure of Isolated U5 snRNP

The 3D structure of U5 snRNP was reconstructed from ~19,300 cryo-negative stain images to a resolution of ~26–32 Å (Figure 2I). The particle measures ~265 Å × 150 Å × 120 Å (Figure 2H). Class averages show many fine-structural features and an excellent agreement

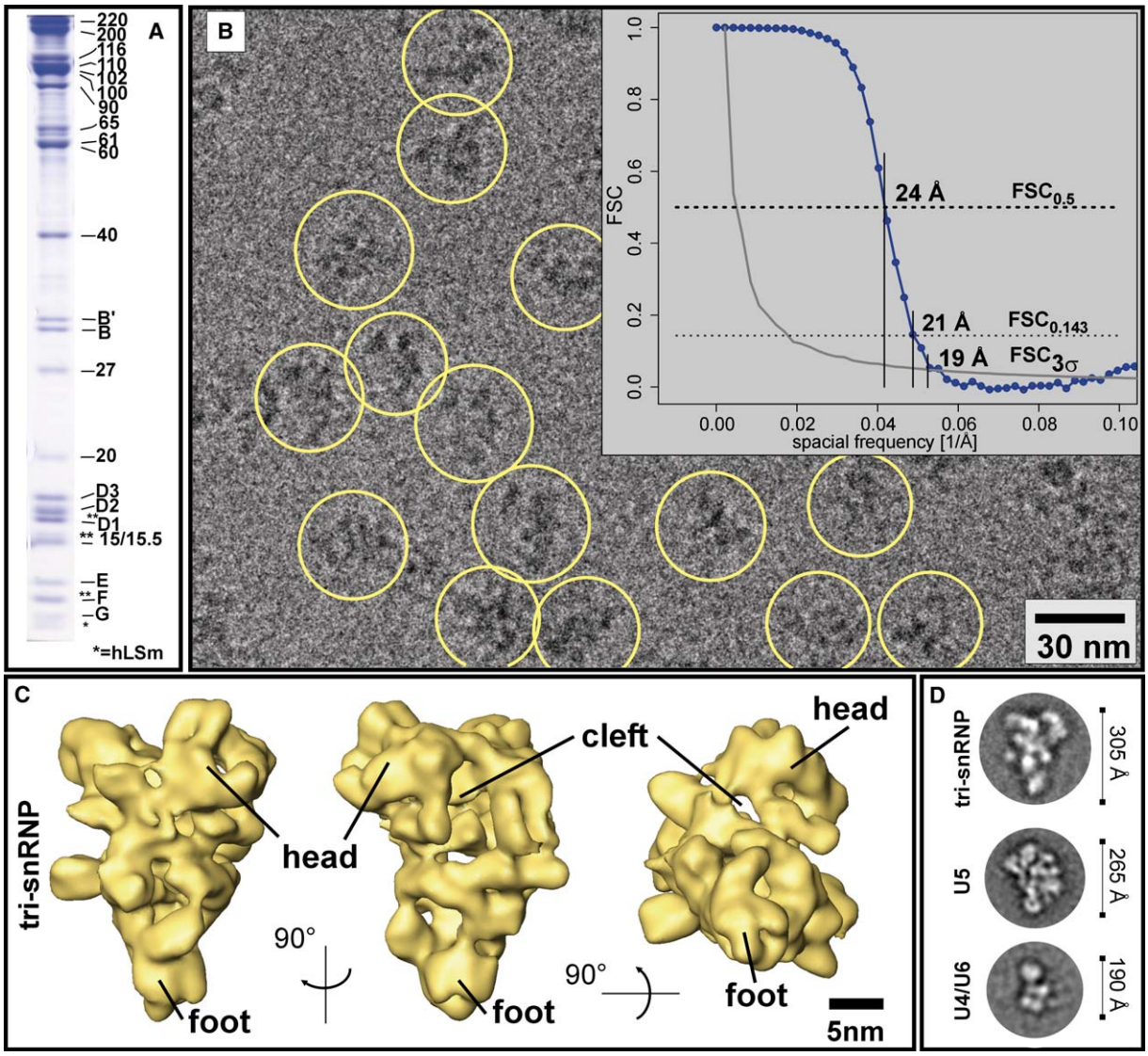

Figure 1. 3D Structure of U4/U6.U5 Tri-snRNP

(A) SDS-PAGE analysis of tri-snRNP showing all tri-snRNP proteins.

(B) Typical electron cryomicrograph with selected particles (in yellow circles), unstained, in vitrified ice. According to FSC analysis (inset), a resolution of 19 Å was obtained by applying the $FSC_{3\sigma}$ criterion, and 24 Å with the $FSC_{0.5}$ criterion (21 Å for both $FSC_{0.143}$ and half-bit criteria).

(C) Three views of the 3D tri-snRNP reconstruction, separated by 90° rotations. The tri-snRNP shows a tetrahedral shape with a broad upper portion and a slim tip at the lower end. At the upper end, a globular, roughly annular domain (head) is separated from the main body by a cleft. As seen in the third panel, the head domain is connected to the main body only by thin linking densities. The maximum dimension of the particle is ~305 Å.

(D) Typical class averages of tri-snRNP, U5 snRNP, and U4/U6 di-snRNP shown on the same scale. In the first panel, cleft and head are visible in the upper right part of tri-snRNP. The convex-concave-shaped U5 snRNP (second panel) is somewhat smaller than the tri-snRNP (~265 Å). In a typical U4/U6 di-snRNP class average, an elongated particle ~190 Å in size with a central constriction becomes visible.

with the corresponding reprojections of the 3D structure (Figure 2G). The U4/U6.U5 and the U5 snRNP possess strikingly similar structural features (see Figures 1C and 2H). The upper domain of U5 snRNP is very similar in size and shape to the head domain of the tri-snRNP and is therefore likewise termed the head domain. As for tri-snRNP, this U5 snRNP head is separated by a cleft from the elongated main body and forms only thin bridges to it. This cleft results in a subdivision of the U5 snRNP into an upper part (one-third) and a lower part (two-thirds). A network of prominent densities is responsible for the roundish, convex-concave shape of the particle. At the lower end of the particle, a globular domain is found that we call the "foot."

3D Structure of Isolated U4/U6 Di-snRNP

The ~3900 U4/U6 di-snRNP particle images obtained were very challenging to analyze at the 3D level because of overall structural heterogeneity. We therefore calculated 118 low-resolution 3D models by the random conical tilt (RCT) method (Radermacher et al., 1987) based upon 118 selected class averages, which we then analyzed by 3D multivariate statistical analysis (MSA) and subsequent classification (van Heel, 1984) of RCT 3D

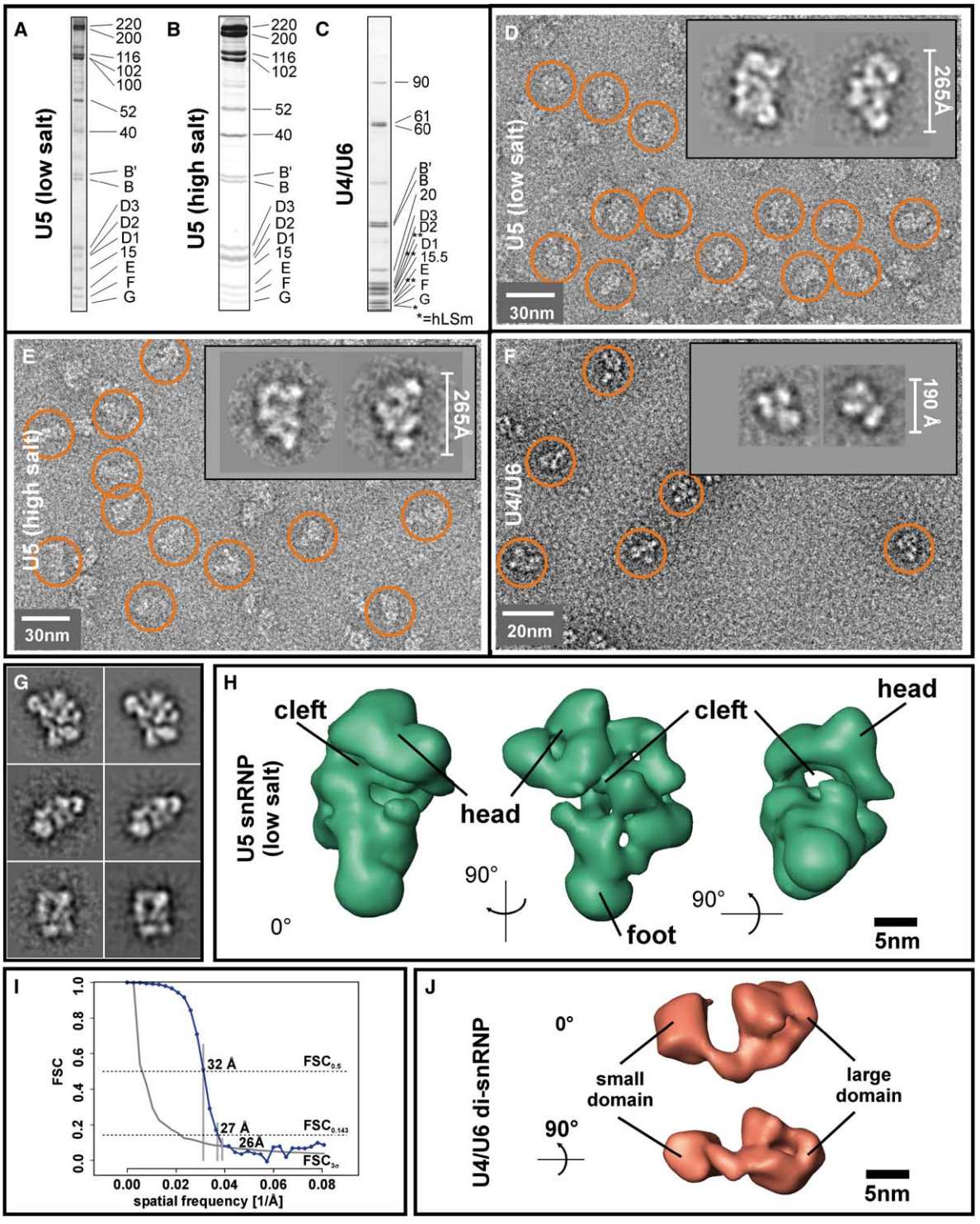

Figure 2. Structural Characterization of the Isolated Tri-snRNP Subunits U5 and U4/U6 snRNPs

(A) The Coomassie-stained gel of isolated U5 snRNPs under low-salt conditions (150 mM NaCl) shows all U5-specific proteins as well as the U5 snRNA-associated set of seven common Sm proteins. The U5-52K represents an additional protein that is absent from the tri-snRNP.

(B) The Coomassie-stained gel of high-salt-resistant U5 snRNP at 800 mM NaCl shows all U5-specific proteins except hPrp28p (which dissociates under high-salt conditions) as well as the common U5 snRNA-associated set of seven Sm proteins.

(C) The silver-stained gel of isolated U4/U6 di-snRNPs shows all U4/U6-specific proteins and the set of U4-associated Sm proteins, as well as the U6-associated set of hLSm proteins.

(D) 2D electron microscopy of negatively stained U5 snRNPs under low-salt conditions reveals a convex-concave-shaped particle 265 Å in size.

(E) When purified under high-salt conditions, the 2D electron-microscopic appearance of the sample is less uniform than in (D), and typical class averages appear slightly slimmer compared with U5 snRNPs under low-salt conditions.

(F) 2D electron microscopy of isolated U4/U6 di-snRNPs. The particles are roughly 190 Å in size and typically exhibit a central constriction.

structures. A typical 3D class average is shown in Figure 2J at the ~40 Å resolution obtained and reveals two globular domains—one larger domain and one smaller domain—connected by a thin bridge with a maximum dimension of ~190 Å. The other 3D class averages exhibited a very similar structure with two unequally sized globular domains connected by a linking density. However, the 3D MSA analysis also revealed different relative positions of the two domains with respect to each other as the main source of heterogeneity, with a maximum diameter varying from ~170 Å to ~210 Å (Figure S3). The higher resolution achieved for tri-snRNP in comparison with its isolated subunits U5 and U4/U6 snRNPs suggests that the tri-snRNP may become structurally stabilized upon assembly.

Rigid-Body Fitting of the Isolated Subunit U5 snRNP into Tri-snRNP

At the level of resolution obtained, it is usually not possible to assign proteins directly by identification of secondary structural elements. For rigid-body fitting of both isolated subunits, we thus applied the following strategy: first, the U5 snRNP was fitted into tri-snRNP based upon the characteristic structural similarities described above, and the quality of the fit was verified by measuring the overlapping portion of voxels. Then, the smaller U4/U6 subunit was fitted on the basis of comparison with the non-U5 part of tri-snRNP, which should represent the U4/U6 di-snRNP (combined mass ~0.5 MDa) plus the three tri-snRNP specific proteins 110K, 65K, and 27K (combined mass ~170 kDa).

U5 snRNP was fitted into the tri-snRNP structure (Figures 3A and 3B) using the main common features head, cleft, elongated main body, and globular foot domain as anchor points. Despite differences in resolution resulting in more fine-structural details in the tri-snRNP compared with the more compact appearance of the U5 snRNP map, the two structures fitted well. Interestingly, a mismatch was found in the U5 head, where only ~40% of the U5 head density was covered by the similarly sized and shaped tri-snRNP head density (Figure 3B, head in blue). However, a movement of the U5 head (rotation of ~30°), which results in a more elongated conformation, leads to a markedly increased correspondence of ~81% (Figure 3C).

Additional Indications for Structural Flexibility of the U5 Head Domain

Experimental indications for flexibility of the U5 head domain came from the 3D analysis of U5 snRNPs under high-salt conditions. As was the case for the U4/U6 di-snRNP images, it proved impossible to merge the complete data set of ~6000 high-salt U5 snRNP images into a common 3D structure. In particular, we first tried to combine 84 RCT 3D reconstructions of high-salt-purified U5 snRNP into a single 3D model, but, owing to significant deviations in the overall curvature of the individual 3D reconstructions, it proved impossible to obtain a single combined 3D structure. The prealigned RCT 3D densities were therefore subjected to 3D MSA and subsequent classification (as were the U4/U6 3D RCT densities described above) into 15 3D classes, four of which are shown (Figure 3D). Densities on the convex side of the low-salt particle are only incompletely observed, leading to a somewhat slimmer appearance of high-salt U5 snRNPs. Most importantly, the U5 snRNP purified in high-salt buffer exhibits considerable flexibility, which is reminiscent of the movement of the head domain described above (Figure 3D). In comparison, the structure of U5 snRNP isolated under low-salt conditions shows a more pronounced overall curvature. Under high-salt conditions, the flexibility of the U5 head domain thus results in further stretching of the U5 snRNP particle, as predicted from the fit of isolated low-salt U5 snRNP into tri-snRNP. Indeed, subpopulations of high-salt-purified U5 snRNP, showing a more elongated conformation, were found that perfectly fitted into the tri-snRNP. Thus, the differences between the various high-salt U5 snRNP structures illustrate a flexion of U5 snRNP that accords with the suggestion that the U5 snRNP head domain moves during assembly of the tri-snRNP.

Further support for the flexibility of the U5 head domain as described here comes from negatively stained tri-snRNP class averages depicting different conformations of the head domain (Figure 3E) and, consistently, from 3D RCT class averages of tri-snRNP showing flexibility of the head domain as the main source of heterogeneity (Figure 3F). On the basis of (1) the improvement of the fit, (2) the flexibility of U5, (3) the flexibility of the tri-snRNP head domain, and (4) the similarity in size and shape of the two head domains, we therefore suggest that the U5 head moves upward upon integration into the tri-snRNP (Figure 3C).

Rigid-Body Fitting of U4/U6 Di-snRNP into the U4/U6.U5 Tri-snRNP

The 3D structure of isolated U4/U6 di-snRNP (Figure 3G) consists of two unequally sized globular domains connected by a linking region and is very similar to the major portion of the so-far-unassigned non-U5 snRNP density (Figure 3H, colored pink). In the fit, the smaller domain of U4/U6 is located in the upper region of tri-snRNP juxtaposed to the head domain, while the larger domain is found in the central region of the tri-snRNP main body. The fit of both U5 and U4/U6 snRNPs into the tri-snRNP density (Figures 3I and 4) finally illustrates the excellent agreement found between these three independently obtained 3D structures. Whereas the U4/U6 snRNP domain is separated from the tri-snRNP head domain by the cleft in the upper part of the tri-snRNP, it forms several close contacts with the central part of the tri-snRNP

(G) Averages of three different views of isolated U5 snRNPs under low-salt conditions (left) together with their respective reprojections from the 3D structure (right), showing excellent agreement.

(H) 3D structure of the U5 snRNP under low-salt conditions with three views separated by 90°. The particle exhibits an elongated, convex-concave shape. Similar to tri-snRNP, an upper globular, roughly annular domain termed head is separated from the body by a cleft.

(I) According to FSC analysis, a resolution of 32 Å was obtained for $FSC_{0.5}$, and 26 Å applying the $FSC_{3\sigma}$ criterion (27 Å for the $FSC_{0.143}$ and 28 Å for the half-bit criterion).

(J) 3D structure of U4/U6 di-snRNPs. Two unequally sized globular domains are connected by a thin linking density.

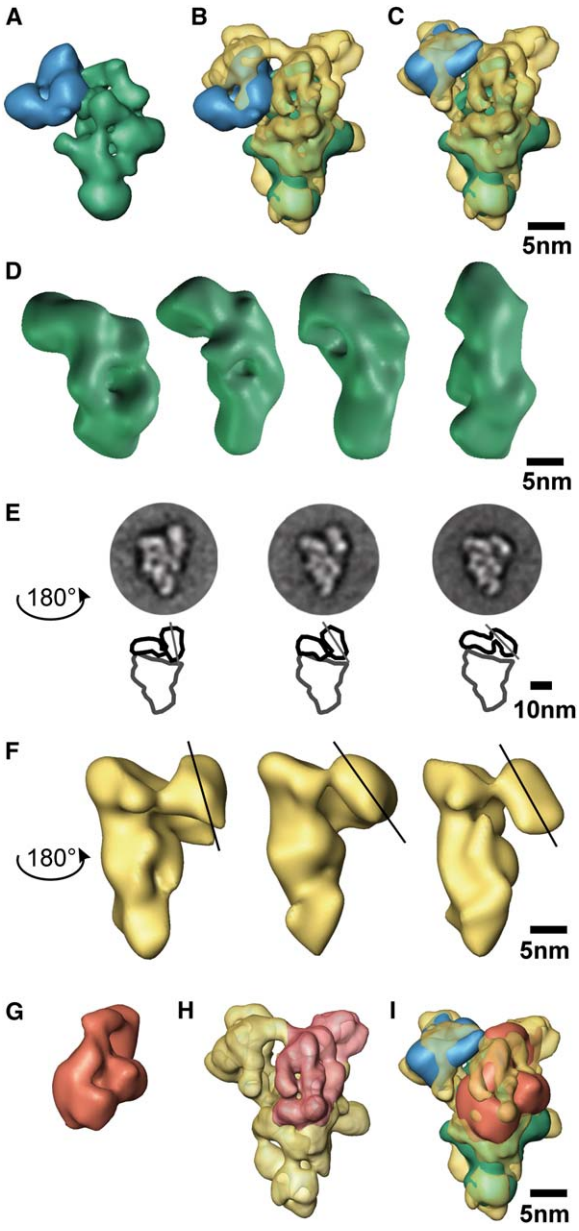

Figure 3. Structural Characterization of the Tri-snRNP

(A) The U5 snRNP is shown from the same direction as in Figure 2H, second column, with the circular head domain in blue and the main elongated body in green.

(B) Rigid-body fitting of U5 snRNP into tri-snRNP (yellow); good fit is observed except for a slight deviation between the head domains.

(C) U5 snRNP particle in the conformation required for integration into tri-snRNP.

(D) 3D structural subpopulations of U5 snRNP purified under high-salt conditions showing different bending as main source of heterogeneity.

(E) Analysis of structural heterogeneity present in tri-snRNP samples, in three class averages (projection view rotated by 180° with respect to [A]–[C]) with almost identical main body but deviations of the head. For illustration, outline plots are shown below.

(F) Tri-snRNP reconstructions revealing at the 3D level that the axis of the head domain constitutes the main source of heterogeneity (view rotated by 180° with respect to [A]–[C].

(G) 3D structure of U4/U6 di-snRNP in the orientation used for fitting into the pink non-U5 snRNP density.

(H) The tri-snRNP density attributed to the U4/U6 di-snRNP (shown in pink).

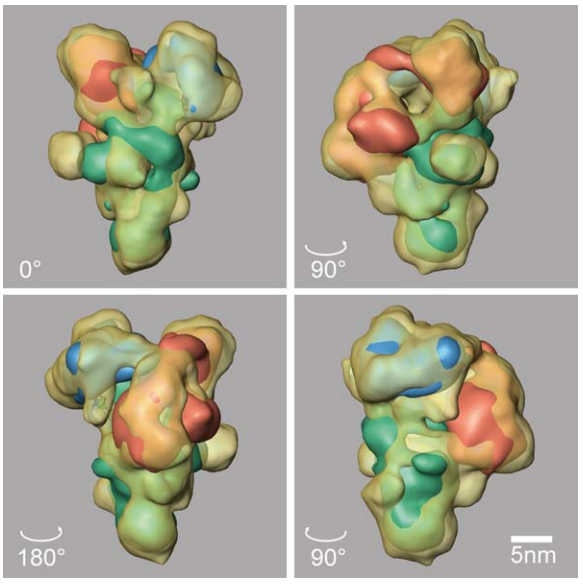

Figure 4. Complete Fit of Isolated U5 and U4/U6 snRNPs into Tri-snRNP

Four views of tri-snRNP filtered to ~3 nm resolution (yellow, semi-transparent) with both isolated subunits fitted into it (green, U5 main body; blue, U5 head domain; red, U4/U6 di-snRNP). The fit reveals the excellent agreement found between tri-snRNP and the independently obtained 3D structures of its two subunits.

main body such that exact borders between the U5 and U4/U6 subunits are not visible in the central part of tri-snRNP. Interestingly, the central part of the main tri-snRNP body that was assigned to the U5 snRNP portion appears to include slightly more density than that of isolated U5 snRNP (the tri-snRNP main body is ~15% larger than its U5 snRNP counterpart). This extra density may account for tri-snRNP-specific proteins (110K, 65K, 27K) not present in the isolated subunits. According to our structural data, these proteins may be located near the interface of the two snRNPs in the region of the main body of the tri-snRNP.

Labeling of U5 snRNA at Loop I and m_3G Cap of U5 snRNP

To locate the functionally important spliceosomal component U5 snRNA loop I, the U5 snRNA of isolated U5 snRNPs was hybridized to a biotinylated 2′-O-allyl-oligonucleotide (Lamm et al., 1991) complementary to loop I. For recognition in the electron microscope, streptavidin was either bound to this complementary oligonucleotide before incubation with U5 snRNPs, or the oligonucleotide label was visualized after binding anti-biotin antibodies to the complexes. Views of labeled U5 snRNP particles were correlated with the U5 3D structure (Figure 5A); importantly, all labeled U5 snRNP views could be unambiguously assigned to different angular views of the U5 snRNP 3D structure. The label consistently revealed the U5 snRNA loop I on the convex side of the central part of U5 snRNP. Control U5 snRNPs

(I) Complete fit is as follows: yellow, tri-snRNP; green, U5 body; blue, U5 head; red, U4/U6 di-snRNP.

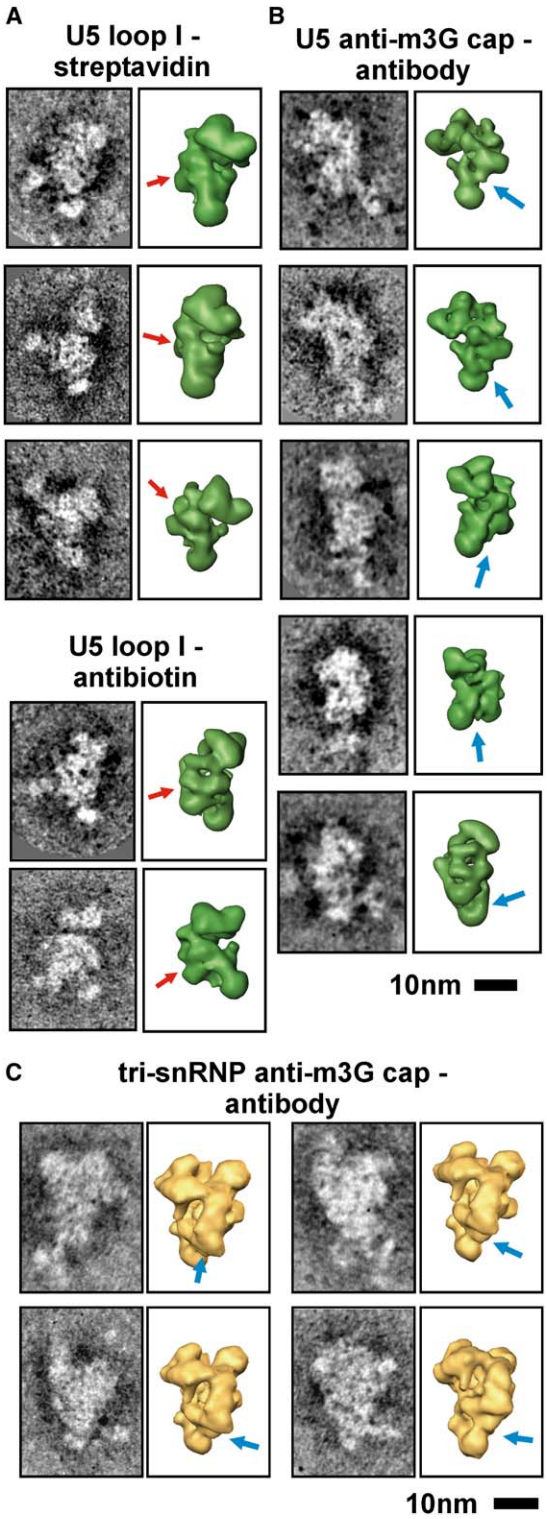

Figure 5. Affinity Labeling of the U5 snRNA in Isolated U5 snRNP and Tri-snRNP

(A) Five selected U5 snRNP particle images, with the biotin-streptavidin or anti-biotin antibody label for the U5 snRNA loop I, are depicted together with the corresponding view of the U5 snRNP structure; the position of the label is indicated by a red arrow.

(B) Five selected U5 snRNP particle images, with the anti-m_3G cap-specific antibody H-20 attached to the 5′ end of the U5 snRNA, are shown together with the corresponding views of the U5 snRNP 3D structure; the position of the label is indicated by a blue arrow.

(C) Four selected tri-snRNP particle images with the anti-m_3G cap-specific antibody H-20 attached to an m_3G cap at the slim lower end of the particle (blue arrow).

plus streptavidin/anti-biotin antibodies without complementary oligonucleotide did not exhibit this additional density. We also correlated anti-m_3G cap antibody-labeled U5 snRNPs prepared essentially as published earlier (Kastner et al., 1990) with the 3D structure of the U5 snRNP (Figure 5B) and determined the center of the consensus region of the U5 snRNA 5′ end at the lower part of the U5 snRNP, ~70 Å below the center of the loop I label. This distance between the centers of the two different U5 snRNA labels as summarized in Figure 6B is consistent with the theoretical, i.e., unkinked, length of the RNA double helices located between loop I and the m_3G cap in the secondary structure model for U5 snRNA (Figure 6A). However, owing to the inevitable inexactness in the assignment of the label position, a kinked course of the U5 snRNA would also agree with our data.

Labeling Studies of U4/U6.U5 Tri-snRNP

Knowing the positions of the m_3G cap and loop I in the U5 snRNP, we can already infer their positions in the tri-snRNP from the rigid-body fit of U5 into tri-snRNP. However, as additional control, we also performed the m_3G cap labeling experiment in the tri-snRNP. In this particle, two specific binding sites for the anti-m_3G cap antibody H-20 are present (i.e., the 5′ ends of the U4 and U5 snRNAs; U6 snRNA contains a different cap), and the accessibility of at least one of these sites is confirmed by the fact that tri-snRNPs can be purified by making use of this antibody. It was therefore expected that H-20 would label either one or both of the snRNA m_3G caps present in the tri-snRNP. Indeed, antibody binding was observed at the lower apex of the tri-snRNP (Figure 5C), consistent with the labeling of isolated U5 snRNP and its fit into the tri-snRNP; we thus infer that this site contains the m_3G cap of U5 snRNA. A second binding site was observed, albeit very rarely, in the region assigned to the U4/U6 snRNP (Figure S4). The excellent agreement between the position of the U5 snRNA m_3G cap in the tri-snRNP as deduced from the fit of U5 snRNP and as determined by direct labeling of tri-snRNP is shown in Figure 6C; this agreement corroborates the fitting of U5 snRNP into tri-snRNP. In contrast to isolated U5 snRNP, the tri-snRNP did not bind radioactively labeled oligonucleotide complementary to U5 loop I (H.B., B.K., and R.L., unpublished data). In view of (1) the fit of the U5 snRNP into the tri-snRNP, (2) the consistent position of the anti-m_3G label in U5 snRNP and in the tri-snRNP, (3) the position of the U5 snRNA loop I in isolated U5 snRNP, and (4) the inaccessibility of U5 snRNA loop I in tri-snRNP, we thus infer that the U5 snRNA loop I in tri-snRNP is located in the center of the tri-snRNP directly behind some U4/U6 density (Figures 6C and 7).

Fitting of Tri-snRNP into the Precatalytic Spliceosome

Finally, we fitted the tri-snRNP density into the 3D structure of the spliceosomal BΔU1 complex (Boehringer et al., 2004) by exhaustive 3D alignment with an initial rotational/translational accuracy of 15°/7 Å. Results with an overlap of voxels of more than 70% were refined in

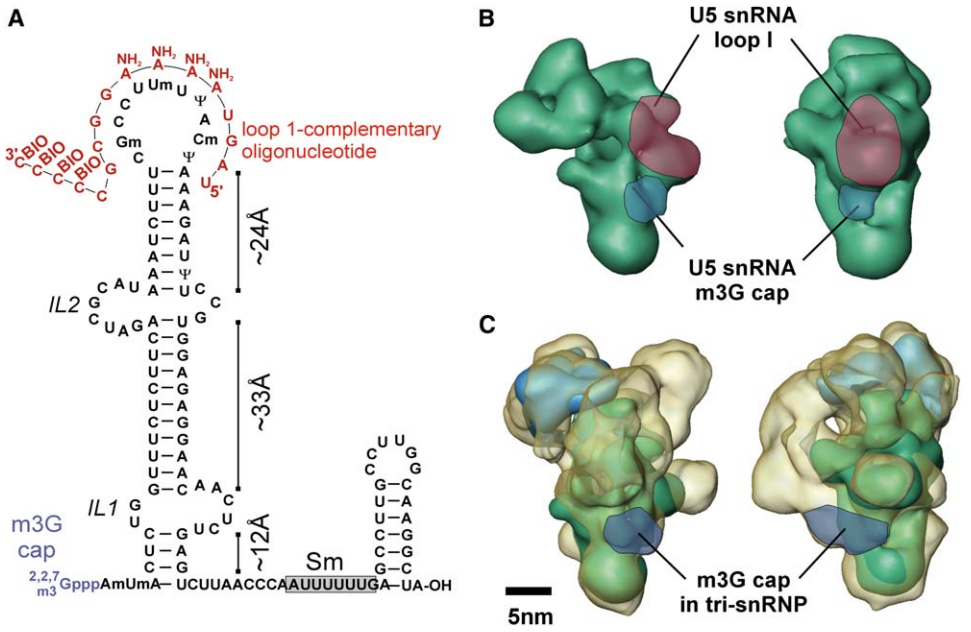

Figure 6. Position of U5 snRNA in Isolated U5 snRNP and Tri-snRNP

(A) Secondary structure of the U5 snRNA. The biotinylated antisense oligonucleotide used for labeling (compare Figure 5A) is indicated in red. Approximate lengths for the double-stranded regions of stem I are shown.

(B) Positions of the labels on the U5 snRNP are red (U5 snRNA loop I) and blue (m_3G cap of U5 snRNA). The centers of the two labeling regions are ~70 Å apart, consistent with the sum of the double-stranded U5 snRNA regions indicated in (A).

(C) Position of the m_3G cap label (dark blue) on the tri-snRNP (yellow), with the U5 snRNP in the same orientation as in (B) (U5 body, green; U5 head, blue). According to the rigid-body fit of U5 snRNP, the two m_3G cap positions in isolated U5 snRNP and tri-snRNP are found at practically identical positions.

a subsequent step, and the five most significant solutions were stored. Then, the U5 snRNA loop I position was transferred to the resulting position in BΔU1, resulting in a central probability cloud shown in Figure 7. Importantly, this probability cloud is located entirely within the central region of the triangular domain of BΔU1, suggesting that this region is the site for the U5 snRNA loop I position within the precatalytic spliceosome.

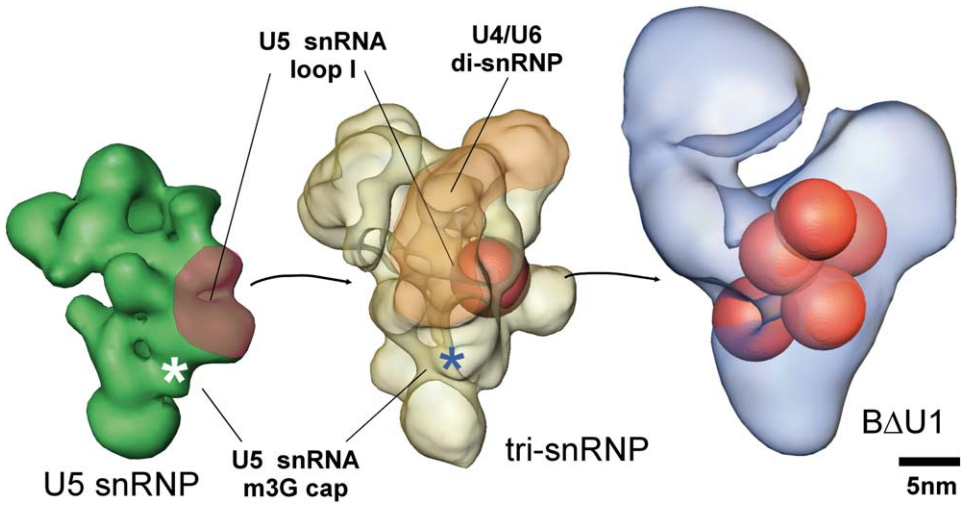

Figure 7. Proposed Model for the Location of U5 snRNA Loop I in Tri-snRNP

By localizing the U5 snRNP subunit within tri-snRNP, a central position of U5 snRNA loop I in tri-snRNP (red sphere fitted into yellow, semitransparent tri-snRNP) in close spatial relationship to the U4/U6 portion (orange area) can be deduced. Fitting of the tri-snRNP 3D structure into the precatalytic spliceosomal complex BΔU1, in which tri-snRNP is bound to the prespliceosome, still produces several fitting possibilities of nearly equal quality. Based upon these fits, the possible positions of the U5 snRNA loop I are shown by red spheres that are clustered in the central region of the spliceosome. We suggest that it is this central region to which the prespliceosomal U2 snRNA comes in close proximity for formation of the spliceosomal catalytic core.

Discussion

We describe herein the 3D structure of tri-snRNP, the largest and most conserved building block of the spliceosome, and of its two subunits U4/U6 and U5 snRNP. By applying fitting procedures, we show how these two subunits combine to form the tri-snRNP and suggest that conformational changes occur in the U5 snRNP subunit when it is integrated into the tri-snRNP. Additional labeling experiments were used to determine the position of two functionally important U5 snRNA sites, 5′ end and loop I, and the RNA locations corroborated the fitting results. Finally, we have determined a consensus region in the precatalytic spliceosome for loop I by exhaustive rigid-body fitting of tri-snRNP.

Proximity of U5 snRNA Loop I and the U4/U6 Portion

The exon-aligning loop I of the U5 snRNA that is supposed to be positioned at the active center in the catalytically active spliceosome was located in the central part of tri-snRNP close to the large globular domain of the U4/U6 di-snRNP subunit. Apart from U5 snRNA loop I, U6 snRNA is known to be located at the catalytic core of the spliceosome and is likely to be involved in the catalysis of splicing (Yean et al., 2000), while U5 snRNA loop I is involved in tethering the exon ends for the splicing reaction (McConnell and Steitz, 2001; Sontheimer and Steitz, 1993; Wyatt et al., 1992). Our data indicate that the functional components (U5 snRNA loop I and U4/U6 snRNAs) may be located near the center of tri-snRNP to support the formation of the spliceosome's catalytic core. An intersubunit border is not visible in this central part of tri-snRNP, and, in view with the presence of non-U5 and non-U4/U6 density in this tri-snRNP region, we therefore suggest that tri-snRNP specific proteins might be located here. This indicates that the organization of this central region depends upon a variety of interactions between the U5 and U4/U6 snRNPs and possibly other tri-snRNP proteins. Indeed, part of the U5 loop I region becomes occluded by the U4/U6 di-snRNP and additional tri-snRNP densities, which is consistent with the failure of the loop I oligonucleotide to bind to the tri-snRNP.

Implications for the Location of the Functionally Important Proteins hPrp8 and U5-116K

The combination of the two U5 snRNA labels together with previous crosslinking data (Urlaub et al., 2000) has implications for the location of hPrp8p. Thus, at least part of hPrp8p should be found in the lower to central region of tri-snRNP in close spatial relationship to loop I and the m_3G cap label. Furthermore, Snu114p, the yeast ortholog of U5-116K, can also be crosslinked to the U5 snRNA (Dix et al., 1998), and thus it may also be found in the central part of tri-snRNP.

Architecture and Flexibility of the U5 snRNP

Our data indicate a movement of the upper U5 head domain upon integration of U5 snRNP into the tri-snRNP; this is based on (1) rigid-body fits of the U5 head into the similarly sized and shaped tri-snRNP head domain, (2) the observed overall flexibility of the U5 snRNP under high-salt conditions, and (3) the flexibility of the head domain in tri-snRNP as observed at the 2D and 3D levels. This movement of the U5 head does not require dramatic conformational reorganization steps in the densities connecting head and body, as these rather thin and filamentous connections are likely to be sufficiently flexible to accommodate the observed movement of the head domain. The U5 snRNP particle under high-salt conditions preferentially adopts a stretched conformation like that observed within tri-snRNP but may also occur in a curved conformation very similar to that observed under low-salt conditions. Thus, molecular interactions within the U5 snRNP that may be needed to maintain a certain position of the head with respect to the main body may be weakened under high-salt conditions. It can therefore be speculated that integration of U5 into the tri-snRNP under physiological salt conditions may require an assembly factor that supports the movement of the U5 head domain. A potential candidate protein shown to be involved in tri-snRNP assembly is the U5-52K protein, which is present in U5 at both salt concentrations but dissociates after tri-snRNP assembly (Laggerbauer et al., 2005).

HPrp28p (U5-100K) is the only protein missing in high-salt-resistant U5 snRNP particles in comparison with low-salt U5 snRNPs (Makarov et al., 2000). One further structural difference between the various conformations of the high-salt-resistant U5 snRNP and the U5 snRNP 3D structure at low salt concentrations is the somewhat slimmer appearance of the main body under high-salt conditions, with less density observed at the convex side of the U5 snRNP particle (compare Figures 2H and 3D). HPrp28p may thus stabilize the convex part, or, alternatively, it may even be located itself in this region of the U5 snRNP particle.

Architecture of U4/U6 Di-snRNP

The U4/U6 di-snRNP consists of two globular domains, the larger one of which is found in very close proximity to the label obtained for the U5 snRNA loop I. This overall appearance is in line with the current structural model of the U4/U6 di-snRNP: the U4/U6 snRNA, involving the stem II and the 5′ stem loop of the U4 snRNA (Figure S3), is known to be associated with most of the U4/U6-specific proteins, including 15.5K, 61K, and the 20K/60K/90K trimeric complex (Nottrott et al., 2002), while the heptameric U6 LSm ring interacts with the nearby 3′ end of U6 snRNA (Achsel et al., 1999). In contrast, the Sm proteins are located in some distance at the 3′ end of U4 snRNA and may be candidates to form a separate small structural domain.

Proposed Site of Formation of the Spliceosomal Catalytic Core

Recently, the 3D structure of the precatalytic spliceosomal complex BΔU1 was determined by electron cryomicroscopy (Boehringer et al., 2004). The triangular body of this complex is reminiscent in size and shape of the tri-snRNP. At present, the exact location of tri-snRNP within the 3D structure of the precatalytic spliceosomal complex BΔU1, which contains all tri-snRNP-specific RNAs, and all proteins except for hPrp28p, is not unambiguous, because of current limitations in the resolution of the 3D structure of BΔU1. Nevertheless, a set of possible fits of tri-snRNP into BΔU1 with almost equal fitting quality reveals several similar solutions. In these fits, all

possible U5 loop I positions that can be deduced from fitting tri-snRNP into this precatalytic spliceosome are clustered in the center of the main triangular body of the precatalytic spliceosome. These putative loop I positions are indicated as red spheres within the 3D structure of the precatalytic spliceosome in Figure 7. Importantly, this probability cloud is located completely within the central region of the triangular domain of BΔU1. Therefore, we suggest that the spliceosomal catalytic core may form likewise in the center of the triangular body of the spliceosome. However, the complete catalytic core requires the prespliceosomal U2 snRNA to approximate to this region and finally to base pair with U6 snRNA. According to our fitting experiments, the flexible upper globular domain of BΔU1 is very unlikely to contain any tri-snRNP density and may thus represent part of the prespliceosomal density that indeed extents toward the center of the BΔU1 triangular main body. We thus suggest that the functionally important components of the prespliceosome (U2 snRNA and pre-mRNA substrate) come in close proximity to the tri-snRNP U6 snRNA and U5 snRNA loop I in the center of the spliceosomal triangular main body during assembly of the catalytically active spliceosome.

All the various components of the spliceosome represent individual structural challenges, and undoubtedly great efforts are needed to characterize these independently in order to combine all results into a complete 4D understanding of the splicing cycle. Structure determination of snRNPs and spliceosomes, analysis of the structural dynamics of purified spliceosomal complexes, and mapping of important functional sites and components, as presented here, will therefore provide a basis for advancing our understanding of the 3D structure and function of the spliceosome as a whole.

Experimental Procedures

Purification of Tri-snRNP and U5 snRNP

Native human 25S tri-snRNPs and 20S U5 snRNPs were isolated from HeLa nuclear extract as described previously (Behrens and Lührmann, 1991): anti-m_3G cap-directed immunoaffinity purification with the m_3G-specific antibody H-20 (Bochnig et al., 1987) was used to obtain a mixture of all snRNP particles; then, glycerol-gradient (10%–30%) centrifugation at 150 mM NaCl was applied to separate the individual snRNPs. All snRNP particles exhibited a defined protein and RNA composition, verified by denaturing gel electrophoresis.

Purification of 13S U4/U6 Di-snRNPs

For isolation of 13S U4/U6 di-snRNPs (Makarov et al., 2000), 25S glycerol-gradient fractions enriched of native tri-snRNPs from HeLa nuclear extract were used as starting material. Tri-snRNP particles were pelleted by centrifugation for 16 hr at 22,000 rpm in a Sorvall S100AT rotor and resuspended in a buffer containing 20 mM HEPES, 200 mM NaSCN, 1.5 mM $MgCl_2$, and 0.5 mM DTT (Achsel et al., 1998). U4/U6 di-snRNPs were separated on a 5%–20% glycerol gradient in a buffer of 20 mM HEPES, 150 mM NaCl, 1.5 mM $MgCl_2$ in a Sorvall TH660 rotor at 34,000 rpm for 15.5 hr.

Labeling of the U5 snRNA in U5 snRNP

Labeling for EM of U5 snRNPs with H-20 antibodies against the m_3G cap was performed essentially as described previously (Kastner et al., 1990). Biotinylated aminoadenosine containing 2′-O-allyloligonucleotide with improved complementarity to the loop I sequence of U5 RNA 5′-U-A-G-U-A(NH_2)-A(NH_2)-A(NH_2)-G-G-C-G-dC(BIO)-dC(BIO)-dC(BIO)-dC(BIO)-U-3′ was kindly provided by Angus Lamond; it was radioactively labeled with γ-[^{32}P]-ATP at its 5′ end by using T4 kinase and thereafter purified by gel filtration with Sephadex G50 (Pfizer/Pharmacia, New York, New York) to remove excess label. Biotinylated 2′-O-allyloligonucleotide (200 pmol) was incubated for 60 min with 400 pmol streptavidin (Pierce, Rockford, Illinois) at 4°C in 70 μl PBS buffer at pH 8.0. The reaction mixture was loaded onto a 2 ml ULTROGEL (LKB/Amersham) AcA column (4 mm in diameter) and eluted with PBS buffer. For binding analysis, 7 μg (~7 pmol) 20S U5 snRNPs were treated with 50,000 cpm (14 pmol) of the radioactively labeled oligonucleotide-streptavidin complex and incubated for 90 min at 25°C in a total volume of 100 μl GP buffer (50 mM Tris-HCl [pH 7.9], 150 mM KCl, 1.5 mM $MgCl_2$, 0.1% v/v NP40). The oligonucleotide-snRNP complexes were analyzed by centrifugation in a Beckman TLS55 rotor at 55,000 rpm for 3.5 hr in a 10%–30% glycerol gradient in GP buffer. The gradients were collected in 100 μl fractions, and the nucleotide content was determined by scintillation counting to verify binding of the oligonucleotide to 20S U5 snRNP particles. For EM labeling with streptavidin (Pierce), 100 μl of the streptavidin-oligonucleotide complex was incubated with 16 pmol 20S U5 snRNPs in GP buffer for 30 min at 30°C followed by 60 min at 0°C (Kastner, 1998). The resulting mixture was subsequently loaded onto a 10%–30% glycerol gradient in GP buffer and centrifuged for 2.5 hr at 4°C in a TLS 55 swing-out rotor at 55,000 rpm. EM labeling with anti-Biotin-antibodies (Sigma) was essentially performed as described for the U5 snRNP anti-m_3G cap labeling (Kastner et al., 1990). U5 snRNP particles labeled with the antisense oligonucleotide were incubated with a 3-fold molar excess of anti-Biotin antibodies for 90 min on ice to allow U5 snRNP-oligonucleotide-antibody complex formation. Then the resulting mixture was loaded on a 10%–30% glycerol gradient in GP buffer. After fractionation, the 20S peak and the region adjacent to the 20S peak were analyzed by negative-stain electron microscopy.

Labeling of the m_3G Cap on 25S U4/U6.U5 Tri-snRNP

Tri-snRNP labeling with H-20 antibody (Bochnig et al., 1987) was performed essentially as described for the U5 snRNP anti-m_3G cap labeling (Kastner et al., 1990). Purified tri-snRNP particles were incubated with a 3-fold molar excess of H-20 antibodies for 90 min on ice to allow tri-snRNP-antibody complex formation. Then the resulting mixture was loaded on a 10%–30% glycerol gradient in GP buffer. After fractionation, the 25S peak and the region adjacent to the 25S peak were analyzed by negative-stain electron microscopy.

Preparation of 25S Tri-snRNPs for Vitrification by Freeze Plunging

25S tri-snRNP fractions were incubated in 0.1% glutaraldehyde overnight. Glycerol was then removed from the buffer by using a desalting spin column (Zeba 0.5 ml, Pierce). For buffer exchange, a glycerol-free but otherwise identical buffer containing 20 mM HEPES, 150 mM NaCl, and 1.5 mM $MgCl_2$ was used. It should be noted that previous attempts to directly elute tri-snRNPs in glycerol-free buffer using immunoaffinity chromatography with immobilized tri-snRNP specific antibodies (against the 110 kDa and the 61 kDa proteins, respectively) resulted in a significant amount of degradation products that made structure determination impossible. In contrast, the procedure applied here was instrumental to obtain unstained cryo-electron micrographs in vitrified buffer of high contrast showing a homogeneous particle population similar to negative-stain electron cryomicroscopy of tri-snRNPs.

Negative Stain Preparations

The specimens were prepared according to a recently published protocol (Golas et al., 2003). A carbon film was floated on the surface of the snRNP particle solution, allowing adsorption over 2 min. The carbon film was then transferred to a second well filled with 2% uranyl formate solution and incubated for 2 min. Subsequently, the carbon film with adsorbed particles was attached to a 400 mesh copper grid on which a carbon film containing holes of ~1–2 μm diameter had previously been mounted. Finally, another carbon film floated onto a second solution of uranyl formate was used to form a sandwich, thus enclosing the specimen in a layer of negative stain. U4/U6 specimens were stored under dry conditions until image acquisition; U5 snRNP and tri-snRNP negative-stain specimens were either stored at room temperature until acquisition of tilt pairs or stored in liquid nitrogen until acquisition of zero-tilt images at approximately −180°C. Glutaraldehyde-fixed specimens were used for 3D

structure determination, and unfixed specimens were used for antibody labeling.

Electron Microscopy

All images for 3D analysis were taken on a Philips CM200 FEG at 200 kV with a TemCam-F415 (TVIPS, Gauting, Germany), while the electron micrographs of labeled snRNPs were obtained on a Zeiss EM 109 at 80 kV (all settings summarized in Table S1). Images taken with the CCD camera were recorded in tile mode and stitched by the EM-Menu software (TVIPS).

Independent Determination of First De Novo 3D Models

Tilted image pairs (−45°/0°) of negatively stained tri-snRNPs, U5 snRNPs, and U4/U6 di-snRNPs were taken. "Reference-free" (Dube et al., 1993) 2D class averages of the untilted images were computed by MSA followed by hierarchical ascendant classification (HAC) using IMAGIC-5 software (van Heel et al., 1996). Initial sets of 50–150 3D models were calculated based on these 2D MSA classes by applying the RCT technique to the tilted images (Radermacher et al., 1987). For each data set, 50–150 3D densities were obtained by using RCT where information about the particles' Euler angles can almost completely be derived from the hardware. To retrieve a first consensus 3D model for each particle representative of the data set, we aligned the individual 3D models by exhaustive 3D alignment via polar coordinates combined with an iterative weighted averaging procedure similar to (Sigworth, 1998). The scheme revealed reproducible representations of the particles that were suitable for further refining using zero-tilted particle images and excellently represented the main particle features (B.S., M.M.G., and H.S., unpublished data).

3D Refinements of U5 snRNP and Tri-snRNP

After correction of zero-tilt images for defocus and astigmatism (Sander et al., 2003a), U5 and tri-snRNP 3D densities were refined by projection matching of zero-tilt particle images. The latter employed corrim-based polar coordinate multireference alignment (Sander et al., 2003b) using fine angular separation of references (2°). Refinement was continued until no further improvement was observed. The resolution was estimated by FSC. For the U4/U6 di-snRNP, 15 MSA-based 3D class averages of an RCT data set comprising 118 RCTs were computed, and a 3D class average representing >75% of the data set was selected for presentation. For the U5 snRNP at high-salt conditions, 84 RCT 3D densities were classified into 15 classes, and four representative classes were chosen for presentation. 3D visualization was performed using Amira 3.1 (TGS, Merignac Cedex, France).

Rigid-body fitting of U5 and U4/U6 snRNPs into tri-snRNP was first performed visually using the landmarks described in the text and then refined by a cross-correlation-based real-space 3D alignment tool. For fitting of tri-snRNP into BΔU1, first an exhaustive alignment with a step size of 15° (rotational) and ~7 Å (translational) was performed, then the best solutions with more than 70% of the tri-snRNP voxels overlapping with BΔU1 voxels were refined with 2° accuracy.

Supplemental Data

Supplemental Data include four figures and one table and can be found with this article online at http://www.molecule.org/cgi/content/full/24/2/267/DC1/.

Acknowledgments

We are grateful to A. Lamond for providing the 2′-O-allyloligonucleotide and to the GBF Braunschweig for HeLa cell cultivation. We thank P. Dube for initializing the 3D analysis; C. Lutz for help with the anti-m_3G labeling experiments; and S.E. Behrens, S. Trowitzsch, G. Weber, and O. Makarova for purification of some of the snRNPs. We thank I. Öchsner, A. Badouin, T. Conrad, P. Kempkes, and H. Kohansal for expert technical assistance. The work was supported by grants from the Bundesministerium für Bildung und Forschung (BMBF) to R.L. and H.S., from the DFG to B.K. and R.L., and the Ernst-Jung-Stiftung and the "Fonds der Chemischen Industrie" to R.L.

Received: May 12, 2006
Revised: July 18, 2006
Accepted: August 22, 2006
Published: October 19, 2006

References

Achsel, T., Ahrens, K., Brahms, H., Teigelkamp, S., and Lührmann, R. (1998). The human U5-220kD protein (hPrp8) forms a stable RNA-free complex with several U5-specific proteins, including an RNA unwindase, a homologue of ribosomal elongation factor EF-2, and a novel WD-40 protein. Mol. Cell. Biol. *18*, 6756–6766.

Achsel, T., Brahms, H., Kastner, B., Bachi, A., Wilm, M., and Lührmann, R. (1999). A doughnut-shaped heteromer of human Sm-like proteins binds to the 3′-end of U6 snRNA, thereby facilitating U4/U6 duplex formation in vitro. EMBO J. *18*, 5789–5802.

Adrian, M., Dubochet, J., Lepault, J., and McDowall, A.W. (1984). Cryo-electron microscopy of viruses. Nature *308*, 32–36.

Azubel, M., Wolf, S.G., Sperling, J., and Sperling, R. (2004). Three-dimensional structure of the native spliceosome by cryo-electron microscopy. Mol. Cell *15*, 833–839.

Behrens, S.E., and Lührmann, R. (1991). Immunoaffinity purification of a [U4/U6.U5] tri-snRNP from human cells. Genes Dev. *5*, 1439–1452.

Bennett, M., Michaud, S., Kingston, J., and Reed, R. (1992). Protein components specifically associated with prespliceosome and spliceosome complexes. Genes Dev. *6*, 1986–2000.

Bochnig, P., Reuter, R., Bringmann, P., and Lührmann, R. (1987). A monoclonal antibody against 2,2,7-trimethylguanosine that reacts with intact, class U, small nuclear ribonucleoproteins as well as with 7-methylguanosine-capped RNAs. Eur. J. Biochem. *168*, 461–467.

Boehringer, D., Makarov, E.M., Sander, B., Makarova, O.V., Kastner, B., Lührmann, R., and Stark, H. (2004). Three-dimensional structure of a pre-catalytic human spliceosomal complex B. Nat. Struct. Mol. Biol. *11*, 463–468.

Das, R., Zhou, Z., and Reed, R. (2000). Functional association of U2 snRNP with the ATP-independent spliceosomal complex E. Mol. Cell *5*, 779–787.

Dix, I., Russell, C.S., O'Keefe, R.T., Newman, A.J., and Beggs, J.D. (1998). Protein-RNA interactions in the U5 snRNP of Saccharomyces cerevisiae. RNA *4*, 1675–1686.

Dube, P., Tavares, P., Lurz, R., and van Heel, M. (1993). The portal protein of bacteriophage SPP1: a DNA pump with 13-fold symmetry. EMBO J. *12*, 1303–1309.

Golas, M.M., Sander, B., Will, C.L., Lührmann, R., and Stark, H. (2003). Molecular architecture of the multiprotein splicing factor SF3b. Science *300*, 980–984.

Golas, M.M., Sander, B., Will, C.L., Lührmann, R., and Stark, H. (2005). Major conformational change in the complex SF3b upon integration into the spliceosomal U11/U12 di-snRNP as revealed by electron cryomicroscopy. Mol. Cell *17*, 869–883.

Harauz, G., and van Heel, M. (1986). Similarity measures between images. Exact filters for general geometry 3D reconstruction. Optik *73*, 146–156.

Hartmuth, K., Urlaub, H., Vornlocher, H.P., Will, C.L., Gentzel, M., Wilm, M., and Lührmann, R. (2002). Protein composition of human prespliceosomes isolated by a tobramycin affinity-selection method. Proc. Natl. Acad. Sci. USA *99*, 16719–16724.

Jurica, M.S., Sousa, D., Moore, M.J., and Grigorieff, N. (2004). Three-dimensional structure of C complex spliceosomes by electron microscopy. Nat. Struct. Mol. Biol. *11*, 265–269.

Kastner, B. (1998). Purification and electron microscopy of spliceosomal snRNPs. In RNP Particles, Splicing and Autoimmune Diseases, J. Schenkel, ed. (Heidelberg, Germany: Springer), pp. 95–140.

Kastner, B., Bach, M., and Lührmann, R. (1990). Electron microscopy of small nuclear ribonucleoprotein (snRNP) particles U2 and U5: evidence for a common structure-determining principle in the major U snRNP family. Proc. Natl. Acad. Sci. USA *87*, 1710–1714.

Kent, O.A., and MacMillan, A.M. (2002). Early organization of pre-mRNA during spliceosome assembly. Nat. Struct. Biol. *9*, 576–581.

Kent, O.A., Ritchie, D.B., and Macmillan, A.M. (2005). Characterization of a U2AF-independent commitment complex (E′) in the mammalian spliceosome assembly pathway. Mol. Cell. Biol. *25*, 233–240.

Laggerbauer, B., Liu, S., Makarov, E., Vornlocher, H.P., Makarova, O., Ingelfinger, D., Achsel, T., and Lührmann, R. (2005). The human U5 snRNP 52K protein (CD2BP2) interacts with U5-102K (hPrp6), a U4/U6.U5 tri-snRNP bridging protein, but dissociates upon tri-snRNP formation. RNA *11*, 598–608.

Lamm, G.M., Blencowe, B.J., Sproat, B.S., Iribarren, A.M., Ryder, U., and Lamond, A.I. (1991). Antisense probes containing 2-aminoadenosine allow efficient depletion of U5 snRNP from HeLa splicing extracts. Nucleic Acids Res. *19*, 3193–3198.

Makarov, E.M., Makarova, O.V., Achsel, T., and Lührmann, R. (2000). The human homologue of the yeast splicing factor prp6p contains multiple TPR elements and is stably associated with the U5 snRNP via protein-protein interactions. J. Mol. Biol. *298*, 567–575.

Makarov, E.M., Makarova, O.V., Urlaub, H., Gentzel, M., Will, C.L., Wilm, M., and Lührmann, R. (2002). Small nuclear ribonucleoprotein remodeling during catalytic activation of the spliceosome. Science *298*, 2205–2208.

McConnell, T.S., and Steitz, J.A. (2001). Proximity of the invariant loop of U5 snRNA to the second intron residue during pre-mRNA splicing. EMBO J. *20*, 3577–3586.

Nottrott, S., Urlaub, H., and Lührmann, R. (2002). Hierarchical, clustered protein interactions with U4/U6 snRNA: a biochemical role for U4/U6 proteins. EMBO J. *21*, 5527–5538.

Radermacher, M., Wagenknecht, T., Verschoor, A., and Frank, J. (1987). Three-dimensional reconstruction from a single-exposure, random conical tilt series applied to the 50S ribosomal subunit of Escherichia coli. J. Microsc. *146*, 113–136.

Sander, B., Golas, M.M., and Stark, H. (2003a). Automatic CTF correction for single particles based upon multivariate statistical analysis of individual power spectra. J. Struct. Biol. *142*, 392–401.

Sander, B., Golas, M.M., and Stark, H. (2003b). Corrim-based alignment for improved speed in single-particle image processing. J. Struct. Biol. *143*, 219–228.

Sander, B., Golas, M.M., and Stark, H. (2005). Advantages of CCD detectors for de novo three-dimensional structure determination in single-particle electron microscopy. J. Struct. Biol. *151*, 92–105.

Sigworth, F.J. (1998). A maximum-likelihood approach to single-particle image refinement. J. Struct. Biol. *122*, 328–339.

Sontheimer, E.J., and Steitz, J.A. (1993). The U5 and U6 small nuclear RNAs as the active site components of the spliceosome. Science *262*, 1989–1996.

Staley, J.P., and Guthrie, C. (1998). Mechanical devices of the spliceosome: motors, clocks, springs, and things. Cell *92*, 315–326.

Teigelkamp, S., Newman, A.J., and Beggs, J.D. (1995). Extensive interactions of PRP8 protein with the 5′ and 3′ splice sites during splicing suggest a role in stabilization of exon alignment by U5 snRNA. EMBO J. *14*, 2602–2612.

Urlaub, H., Hartmuth, K., Kostka, S., Grelle, G., and Lührmann, R. (2000). A general approach for identification of RNA-protein cross-linking sites within native human spliceosomal small nuclear ribonucleoproteins (snRNPs). Analysis of RNA-protein contacts in native U1 and U4/U6.U5 snRNPs. J. Biol. Chem. *275*, 41458–41468.

van Heel, M. (1984). Multivariate statistical classification of noisy images (randomly oriented biological macromolecules). Ultramicroscopy *13*, 165–183.

van Heel, M., Harauz, G., Orlova, E.V., Schmidt, R., and Schatz, M. (1996). A new generation of the IMAGIC image processing system. J. Struct. Biol. *116*, 17–24.

Will, C.L., and Lührmann, R. (2006). Spliceosome Structure and Function, Third Edition (Cold Spring Harbor, New York: Cold Spring Harbor Laboratory Press).

Wu, J.A., and Manley, J.L. (1991). Base pairing between U2 and U6 snRNAs is necessary for splicing of a mammalian pre-mRNA. Nature *352*, 818–821.

Wyatt, J.R., Sontheimer, E.J., and Steitz, J.A. (1992). Site-specific cross-linking of mammalian U5 snRNP to the 5′ splice site before the first step of pre-mRNA splicing. Genes Dev. *6*, 2542–2553.

Yean, S.L., Wuenschell, G., Termini, J., and Lin, R.J. (2000). Metal-ion coordination by U6 small nuclear RNA contributes to catalysis in the spliceosome. Nature *408*, 881–884.

Accession Numbers

The EM maps have been deposited at the EMDB database under the accession numbers EMD-1257, EMD-1258, and EMD-1259.